Lasers in Manufacturing Conference 2019

Numerical simulation of residual stresses in laser welding: application to Ti6Al4V/316L steel assembly with vanadium insert

Antoine Mannucci[a,b], Rodolphe Bolot[a][*], Alexandre Mathieu[a], Iryna Tomashchuk[a], Eugèn Cicala[a], Cyril Roudeix[b], Sébastien Lafaye[b]

[a]*Laboratoire Interdisciplinaire Carnot de Bourgogne, UMR 6303 CNRS, Université de Bourgogne Franche-Comté, 12 rue de la Fonderie, 71200 Le Creusot, France*
[b]*Laser Rhônes-Alpes, 49-51 Boulevard Paul Langevin, 38600 Fontaine, France*

Abstract

Prediction of residual stresses in laser welding is an important challenge allowing better understanding of forces involved in the bonding strength mechanisms. This type of simulation is particularly complementary with measurements. Direct welding of titanium to stainless steel is challenging due to the formation of brittle intermetallic compounds. A good strategy to solve this problem consists in using a compatible insert material. The case of laser welding with vanadium insert was thus considered in the present work. A FEM model was developed to simulate the two-step welding process (titanium/vanadium weld followed by vanadium/steel weld). The case of 1 mm thick plates with a 2 mm large vanadium insert was considered to avoid any contact between the two welds. A semi-coupled model was developed: the thermal problem considering equivalent heat sources is solved in a first step, and the mechanical problem in a second one. A complete cooling of the titanium/vanadium assembly is considered before manufacturing of vanadium/steel weld.

Keywords: dissimilar welding ; numerical simulation ; FEM ; stainless steel ; titanium ; vanadium;

* Corresponding author. Tel.: +33-38-573-1042; fax: +33-38-573-1120.
E-mail address: rodolphe.bolot@ubfc.fr

1. Introduction

Laser welding of titanium alloys to stainless steels is of high interest for chemical, medical and aeronautical industries. However, fusion joining of this dissimilar couple of materials remains challenging because of formation of brittle intermetallic compounds such as Fe_2Ti, FeTi and $Cr_7Fe_{17}Ti_5$. An efficient solution for avoiding cold cracking produced by these phases due to thermal strains is to modify the chemistry of the melted zones by introducing an intermediate material compatible with titanium and stainless steel at once. Among compatible materials, vanadium is certainly the best candidate for applications in which biocompatibility is not concerned (Tomashchuk and Sallamand, 2018). The analysis of available literature (Adomako et al. 2019, Adomako et al. 2018,Tomashchuk et al. 2015) shows that the embrittlement of this dissimilar combination can be efficiently avoided by applying two pass joining, when the vanadium insert is first welded with titanium alloy and then with stainless steel.

In dissimilar welding, the problematics of residual stresses is of high concern, because of existing mismatch in thermophysical properties, and contraction of the melted material during cooling after solidification. Undesirable stresses and deformations are even more pronounced in case of joining of thin sheets with butt configuration (Bajpei et al. 2016). In the last years, finite element modeling of the thermomechanical behavior during fusion dissimilar welding is actively developing (Bajpei et al. 2016, Abburi Venkata et al. 2016, Hartel at al. 2016). It involves sequential calculation of the heat flow problem (using equivalent source approach), and the mechanical one (strains and stresses) during and after the welding operation.

This work was carried out in parallel with PhD thesis of A. Mannucci (Université de Bourgogne Franche-Comté, FR), performed in partnership with French SME LRA (Laser Rhône-Alpes). The main technological aim of this project is to define optimized welding conditions allowing titanium/steel assembly with a high bonding strength. Since brittle intermetallic compounds are formed in case of direct welding (Mannucci et al. 2018), an intermediate vanadium insert was used. Thermo-mechanical modeling of strains and stresses associated to the weld operation was thus applied in parallel, to deepen the understanding of phenomena involved in welding process and bonding mechanisms.

2. Experimental results

The case of welding of one-millimeter thick plane sheets with a two-millimeter wide vanadium insert was considered. A TRUMPF TRUDISK 6001 laser was used to manufacture the welds, with moderate laser power range, and a 100 µm diameter optical fiber allowing providing narrow welds. The assembly was manufactured in two steps: the first one consisted in manufacturing a weld in between Ti6Al4V alloy and vanadium, and the second one a weld in between vanadium and 316L stainless steel. Table 1 summarizes experimental conditions for these two welds.

Table 1. Experimental conditions used to manufacture Ti/V and V/SS welds

	Ti6Al4V/vanadium	Vanadium/316L
Linear energy (J/mm)	6.8	10
Spot size (µm)	100	100
Beam offset (µm)	0	50 (316L side)

Figure 1 shows cross-sections of the two welds. The first picture (left) shows the microstructure of the Ti6Al4/vanadium weld. In this picture, the titanium alloy is at the left side and clearly shows a ZAT with a

width of about 200 μm. The width of the weld is about 235 μm (middle), 650 μm (top), and 390 μm (bottom). Due to the differences in the melting temperature (1910°C for vanadium, against 1650°C for Ti6Al4V), and laser light absorption, the chemical composition of the weld was found to be slightly staggered in the titanium side (i.e., V element content of about 33 % in the weld despite the absence of beam offset for this weld). The right picture shows the microstructure of the assembly for the vanadium/SS316L side. In this picture, the vanadium is at left and stainless steel is at the right side (i.e., with coarser grains). The width of this weld is about 240 μm (middle), 425 μm (top), and 320 μm (bottom). Due to the staggering between the laser scan and joint plane (i.e., beam offset of 50 μm on the 316L side), the chemical composition of the weld is significantly staggered in the stainless steel side (i.e., vanadium element content of about 11% only in the weld). Please also note that the height of this second weld is about 840 μm only, which might contribute to lower the bonding strength. More details about the experimental part of the study are provided in article by Mannucci et al. *Pure vanadium insert for efficient joining of Ti6Al4V to 316L stainless steel with continuous Yb:YAG laser,* LIM 2019.
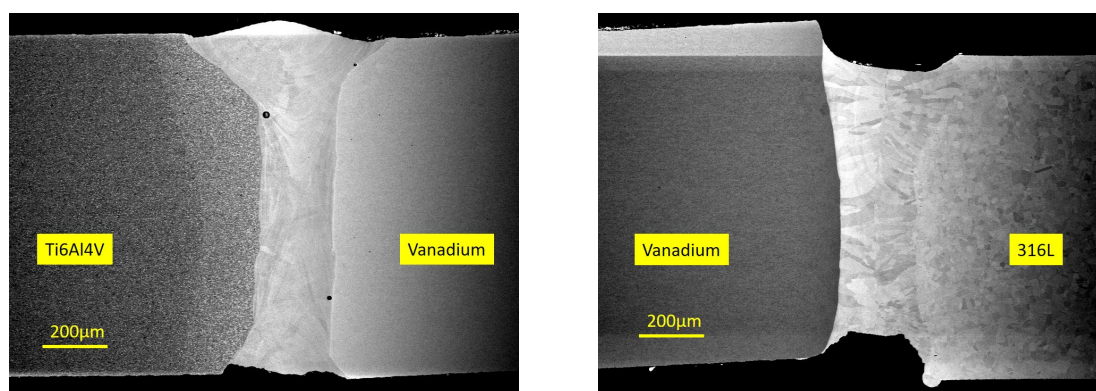

Fig. 1. (a) Ti6Al4V/vanadium weld (left), (b) vanadium/SS316L weld (right)

3. Numerical models

The main objective of the present linked article is to show some results obtained by FEM modeling, corresponding to the same experimental conditions. Two different models developed with ANSYS APDL were applied to this experimental case. The first one consists in a macroscale model with an element size of 50 μm or more (mesh resolution of 100 μm for the coming results).

3.1. Macroscale model

This first model is three-dimensional and designed to study the transient thermomechanical behavior of the assembly during the welding process. It is semi-coupled, meaning that the thermal problem is solved first, whereas the mechanical one is solved in a second step, considering the large deformations option. The coming results were obtained with a mesh resolution of 100 μm for both X and Y directions (200 μm along the Z direction, which is that of the weld axis). In addition, the case of two sheets with dimensions of 20x20 mm was considered. These two sheets were separated by a two-millimeter wide vanadium insert (as for the experiments). Finally the model incorporates 120 000 elements for a little less than 135 000 nodes. Figure 2 shows the mesh whose elements are composed of perfectly squared bricks. In the X direction (transverse vs. the welds), a four-millimeter wide region with homogeneous mesh size is considered (i.e., whole vanadium

region + one-millimeter wide region in the Ti6Al4V and stainless steel directions). Beyond a distance of one millimeter from the welds, a progressive increase of the mesh size is used (with a mesh size increasing according to a geometrical law). Many FEM models suggested in the literature consider formerly connected materials and are used to compute the effect of a remelting of the material in the weld (or welds). In the current model, this is not the case and the different materials are not connected beforehand, but separated by a layer of deactivated elements (white lines on the figure). In other words, a layer of elements is formerly killed (feature of death and birth of elements). This method thus requires the elaboration of welding spots (such as it is done experimentally). In particular, two welding spots are thus first manufactured for each weld (beginning and end of each weld).
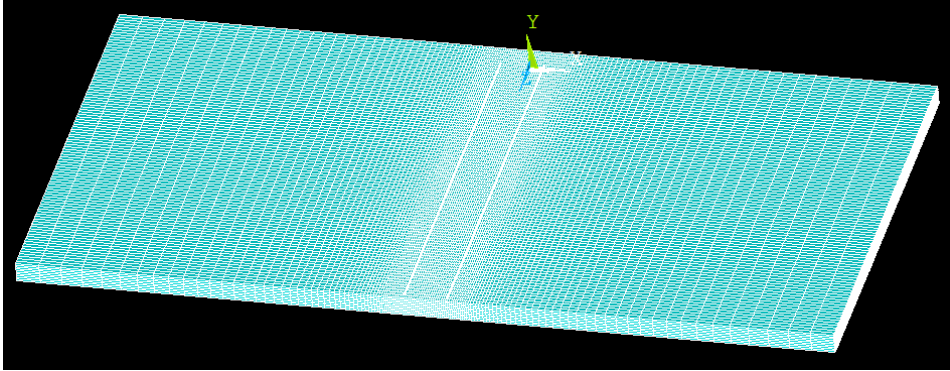

Fig. 2. View of the 3D mesh used in the first model (three-D transient thermomechanical model with 120.000 elements)

The formerly killed elements are thus progressively reactivated (`ealive APDL command`) during manufacturing of the welds. In practice, the model considers not three, but five distinct materials (i.e., Ti6Al4V, vanadium, 316L, but also the two distinct welds). Stainless steel 316L is at the left side of Fig. 2 (i.e., negative X) whereas Ti6Al4V is at the right side (positive X). The two-millimeter vanadium insert corresponds to the part between the two white lines (i.e., positions of the two welds).

In order to simplify the coding of materials properties (and in view of the lack of properties of the corresponding mixed materials), the properties of the welds were considered as follows:
- Ti6Al4V/vanadium weld: Ti6Al4V properties except for the reference temperature used to set the thermal strain
- 316L/vanadium weld: 316L properties except for the reference temperature used to set the thermal strain

In other words, it is assumed that the reference temperature of Ti6Al4V and 316L sheets is the ambient temperature (same for the vanadium insert also). However, the reference temperature of the material of the Ti6Al4V/vanadium weld was set to 1650°C, and that of the 316L/vanadium weld was set to 1400°C.

By doing so, the thermal strain ε_T is thus computed from:

$$\varepsilon_T = \int_{T_{ref}}^{T} \alpha dT = \bar{\alpha} \left(T - T_{ref} \right) \qquad (1)$$

as soon as the welds are progressively manufactured.

This method allows taking into account the materials contraction during cooling from the melting temperature to the ambient one. Concerning the expansion coefficients, either the instantaneous (namely α) or average (namely $\bar{\alpha}$) coefficient can be provided. Within ANSYS, the instantaneous coefficient is stored in

variable named CTEX whereas the average one is named ALPX. It is important to understand that α does not depend on the reference temperature T_{ref} (but that $\bar{\alpha}$ does).

3.2. Microscale model

One of the expertise field of our team concerns calculation on microstructures. This type of calculations may be used to estimate effective properties of porous or multicomponent materials, according to the methods described for example by Bolot et al., 2017. In the present work, calculations were conducted directly on the micrograph of the assembly in order to investigate residual stresses linked to thermal strains in the welds. Figure 3 shows the cross-section of the assembly after reconstitution. In this example, the considered resolution was about 320 pixels/mm (i.e., 3.1 µm/pixel). This value can be compared to that of the first model (i.e., 100 µm/element). Using this type of simulation, the mesh is directly formed by the pixels of the image.
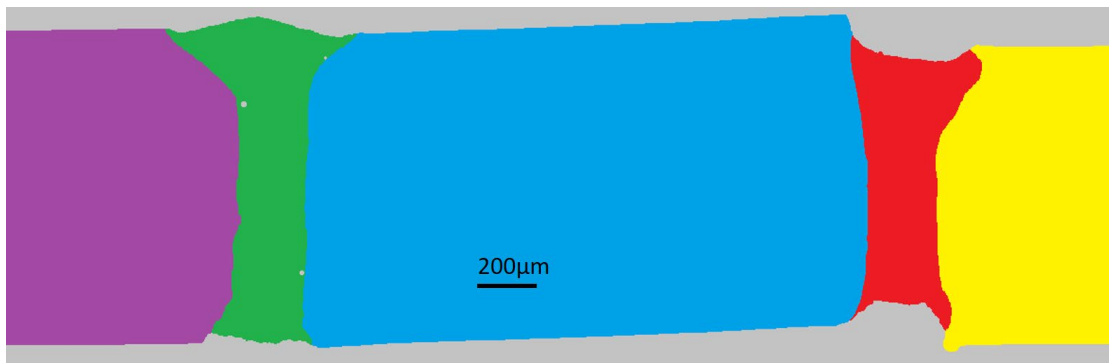

Fig. 3. View of the 2D mesh used in the second model (2-D stationary thermomechanical model with about 440.000 elements)

In fact, images are really efficient meshes, with perfectly square elements (pixels). However, up to now, 3D transient calculations are not possible at this resolution level. In practice, an in-house conversion program is developed, allowing converting images in a corresponding APDL script (readable by ANSYS). With this tool, a 2D mesh is automatically generated from the considered image, with as many materials as there are different colors in the image.

In this example, six different materials are thus considered: from the left to the right Ti6Al4V (1, purple), first weld (2, green) including pores, vanadium insert (3, blue), second weld (4, red) and stainless steel (5, yellow). The last material stands for the grey color around the assembly: the corresponding material has low properties (i.e., such as a Young modulus of 0.1 MPa in practice), or the corresponding elements may alternatively be killed (as done in the present work).

4. Numerical results

4.1. Macroscale model

Figure 4 shows the transient temperature field obtained during manufacturing of the second weld (316L/vanadium weld). Concretely, this weld was manufactured after complete cooling of the first one. The transient position of the laser is 15 mm from position Z=0 for a plate dimension of 20 mm. One may notice that according to the color scale, the melting temperature of 316L (about 1400°C, i.e., 1673 K) corresponds to the orange color on Fig. 4.
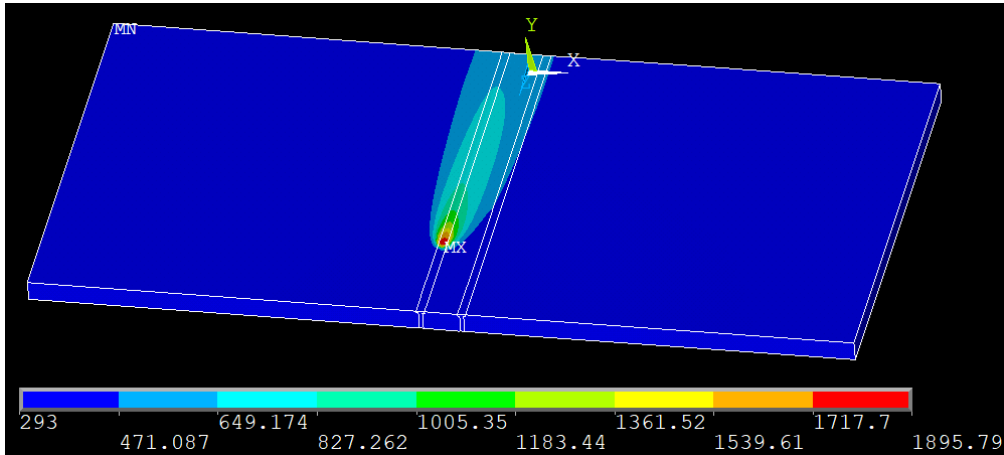
Fig. 4. Transient temperature field (K) during manufacturing of the 316L/vanadium weld (i.e., the second one).

All results presented hereafter concern results after manufacturing of the two welds, and cooling of the assembly down to the ambient temperature (i.e., residual stresses for stress representations). Figure 5 shows the X displacement field Ux (X being the transverse direction regarding the vanadium insert). During manufacturing of the welds, the boundary condition at the two faces X=±L were set as Ux=Uy=Uz=0. However, the boundary condition at the right side (i.e., X=+L) was released after manufacturing of the welds (but the left one was maintained). For this reason, the residual X displacement is almost 0 (yellow color) for the stainless steel sheet (left side). On the contrary, due to the contraction of the welds, the X displacement of the right sheet (Ti6Al4V) is slightly negative (i.e., about -300 μm). Figure 6 shows the Y displacement field Uy this time. The Y displacement is almost 0 (blue color) for the whole stainless steel sheet. On the contrary, since the welds are wider on the top face, their contraction is higher at the top side, so that they provide a small angle of the Ti6Al4V sheet (i.e., Y displacement of 235 μm at the right side of the assembly (red color)).
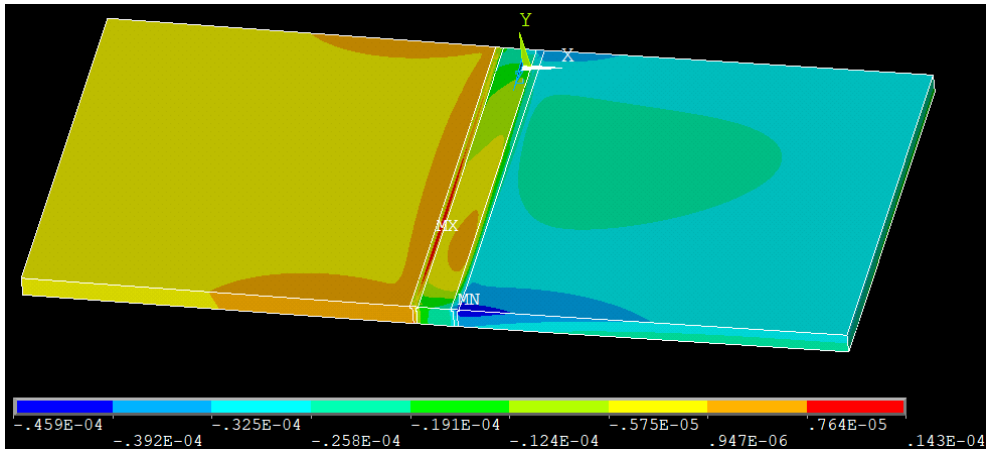

Fig. 5. X displacement field Ux (m) after overall cooling down, and release of the boundary condition at the right face.

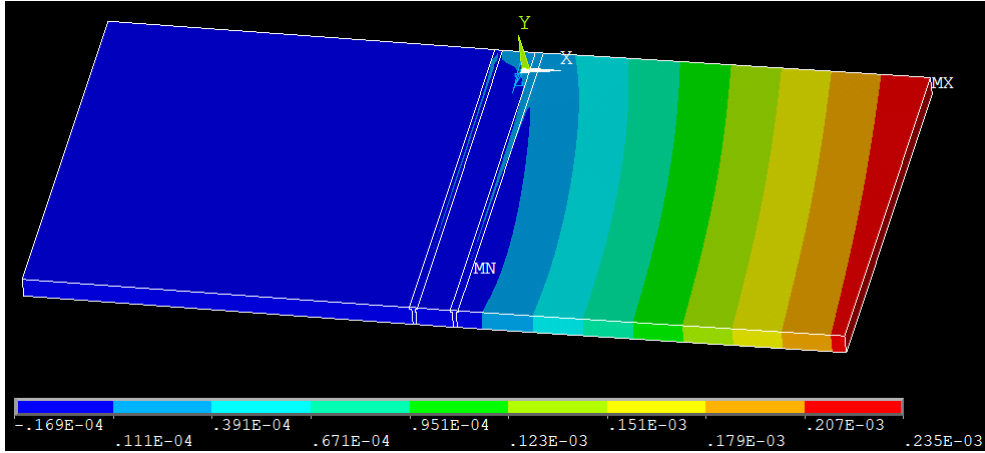Fig. 6. Y displacement field Uy (m) after overall cooling down, and release of the boundary condition at the right face.
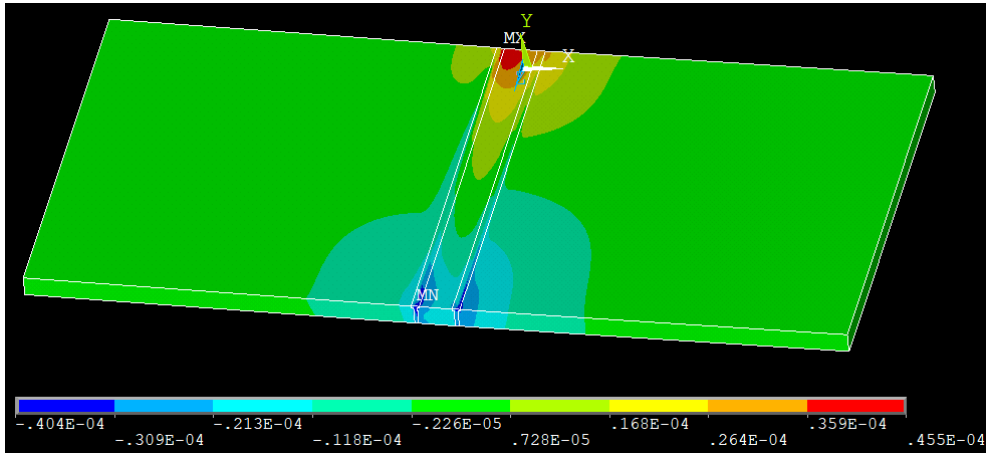

Fig. 7. Z displacement field Uz (m) after overall cooling down, and release of the boundary condition at the right face.

Figure 7 shows the last displacement field (i.e., that in the Z direction, Z being the direction of the axis of the welds). The Z displacement is almost zero (green color) in the whole assembly. However, due to the contraction of the welds, the Z displacement is positive (red color) at Z=0 and negative (blue color) at Z=+L in the vicinity of the welds, and particularly in the vanadium insert. Figure 8 shows the field of thermal strain (see equation (1)) in the assembly. The thermal strain is zero in the two sheets and in the vanadium insert, since $T = T_{ref}$=293 K for these three parts. However, due to the cooling from the melting temperature to the ambient one, the thermal strain is negative in the two welds (i.e., contraction). Figure 9 shows the field of the residual Von Mises plastic strain. In practice, the contraction due to the thermal strain ε_T is offset (or balanced) by a mechanical strain occurring mainly in the welds and their vicinity (i.e., the contraction of the welds provides a contraction of materials in the vicinity of the welds). Figure 10 shows the field of residual X component of stresses (σ_x). The X stress component σ_x is almost zero (clear green color = from -103 to +46 MPa). However, the X stress σ_x is negative in the two welds (i.e., green color, σ_x from -253 to -103 MPa). These negative values in the welds are balanced by positive values (yellow color, σ_x from +46 to +196 MPa) in the vicinity of the welds, and at Z=0 and Z=+L boundaries.
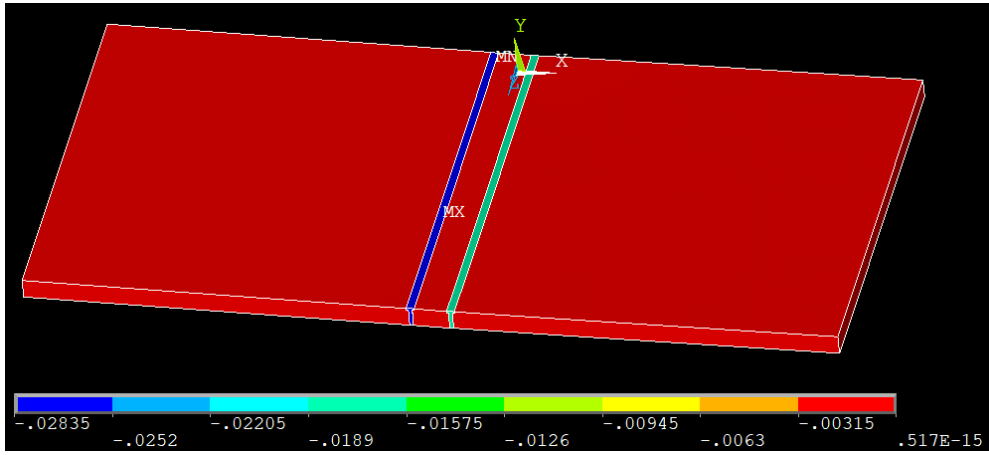
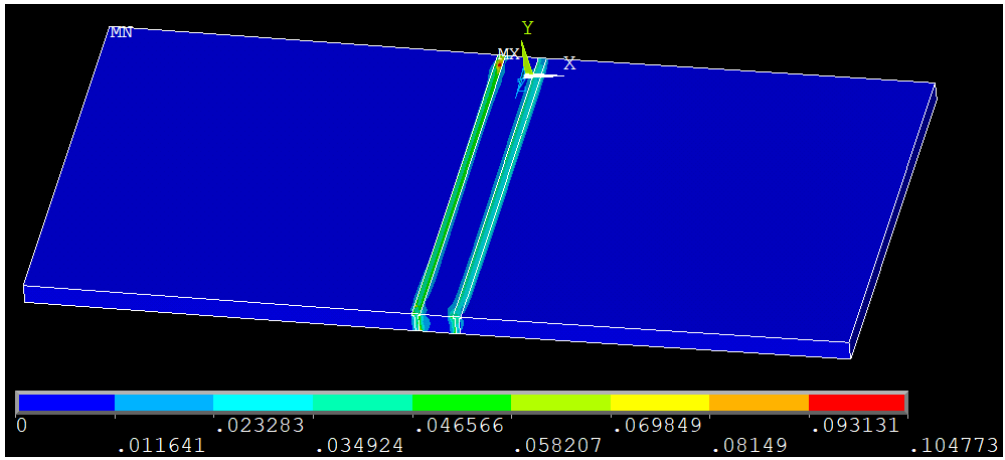Fig. 8. Field of thermal strain ε_T after overall cooling down.

Fig. 9. Field of the Von Mises plastic strain after overall cooling down.
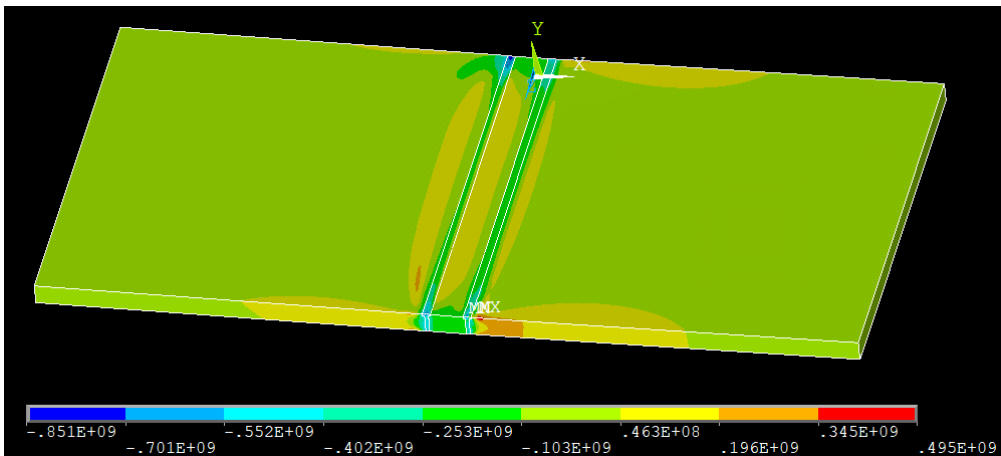

Fig. 10. Field of residual X component σ_x (Pa) of the stress tensor.

Figure 11 shows the field of residual Z component of stresses (i.e., σ_z component in the direction of the axis of the welds). The σ_z component is positive (i.e., tensile stress) in the two welds with a magnitude comprised between +640 and +780 MPa (orange color). This positive σ_z component of the stress tensor in the welds is balanced by a negative component in the two sheets. In the 316L sheet, the σ_z component remains positive (clear green color σ_z from +359 to +500 MPa) just in the vicinity of the weld and become negative (second blue color from -66 to -208 MPa at a distance higher than 2 mm from the weld. In the Ti6AlV4 sheet, the transition from a positive component in the weld to a negative value in the Ti6Al4V sheet, occurs much faster and the negative component in the sheet shows a higher magnitude (dark blue color from -200 to -350 MPa). Figure 12 shows the resulting Von Mises residual stress. The Von Mises stress is low in the two sheets (dark blue color from 0.12 to 114 MPa). It seems also quite low in the vanadium insert. In fact, the highest resulting Von Mises stress is located in the welds (orange color from 800 to 900 MPa).
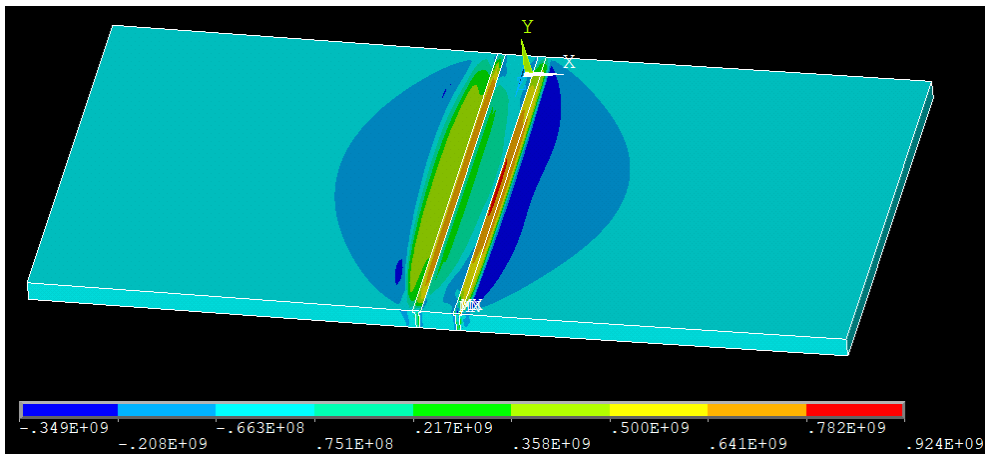

Fig. 11. Field of residual Z component σ_z (Pa) of the stress tensor.
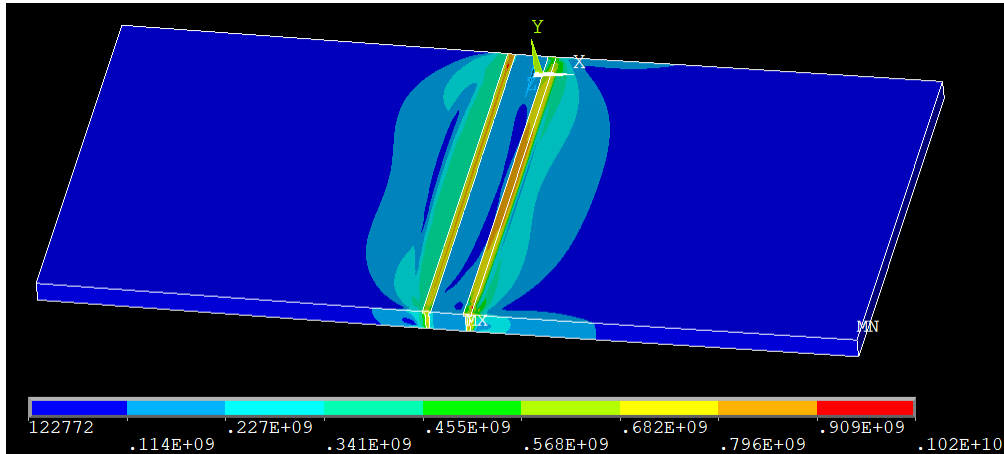

Fig. 12. Field of the Von Mises residual stress (Pa).

4.2. Results from the microscale model

Figure 13 shows an example of result calculated with the microscopic-scale model. In the present calculation, the thermal strain in the welds was set with a reference temperature of 60% of the temperature difference between the melting temperature and the ambient one (i.e., $T_{ref} = 293 + 0.6\,(T_m - 293)$). In practice, values of 830°C (SS316/vanadium weld) and 1000°C (Ti6Al4V/vanadium weld) were thus applied for the reference temperature in the two welds (see equation 1). According to the microscale model, the stress level is thus higher in the Ti6Al4V/vanadium weld, which is mainly due to the higher yield stress of the titanium alloy (i.e., about 1 GPa for Ti6Al4V titanium alloy against less than 350 MPa for 316L stainless steel). It is thus obvious that the results become sensitive regarding to the way the materials properties of the welds are set. One recall here that the mechanical properties of the welds were set to those of Ti6Al4V (first weld) and 316L steel (second weld).
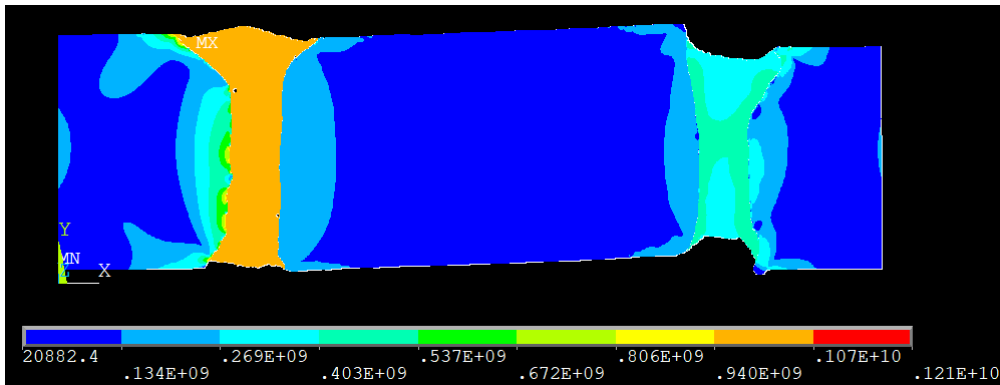

Fig. 13. Von Mises residual stress (Pa) computed with the microscale model (resolution of 3 μm).

5. Conclusions

This work was intended to provide complementary information about a dissimilar assembly performed by laser welding using an insert material. More precisely, a plane sheet of 316L stainless steel was assembled to a titanium sheet using a vanadium insert. The corresponding experimental results are proposed in another associated article (same conference, see article by A. Mannucci et al.), and this work was more devoted to show correlated modeling results. Two different models were applied. The first one was built at a macroscopic scale with a mesh resolution of 100 μm: this model is three-dimensional and transient, and allows the prediction of residual stresses in the assembly, as well as all the transient behavior during manufacturing of the welds. The second one (microscopic model) uses directly the micrograph of the cross-section of the assembly as mesh, with a resolution of about 3 μm. In this second model the mesh is the micrograph (i.e., one element par pixel), and six different areas (materials) were considered (namely 316L steel, vanadium, Ti6Al4V the two welds, and the surrounding environment whose the corresponding elements are formerly killed). Estimations of residual stresses linked to thermal strains were performed using this model, by considering the contraction of the welds during cooling down after solidification. Complementary results (strain components and stress components) will be shown during the conference. Nevertheless, it is emphasized that the results are sensitive regarding to the constitutive law applied for materials, so that an uncertainty remains, especially regarding the magnitude of the stress components.

Acknowledgements

References

Tomashchuk, I., & Sallamand, P., 2018. Metallurgical strategies for the joining of titanium alloys with steels. Advanced Engineering Materials, 20(6), p. 1700764.

Adomako, N. K., Kim, J. O., & Kim, J. H., 2019. Microstructural evolution and mechanical properties of laser beam welded joints between pure V and 17-4PH stainless steel. Materials Science and Engineering: A 753, p. 208.

Adomako, N. K., Kim, J. O., Lee, S. H., Noh, K.-O., Kim, J. H., 2018. Dissimilar welding between Ti–6Al–4V and 17-4PH stainless steel using a vanadium interlayer. Materials Science & Engineering A 732, p. 378.

Tomashchuk, I., Grevey, D.,Sallamand, P., 2015. Dissimilar laser welding of AISI 316L stainless steel to Ti6–Al4–6V alloy via pure vanadium interlayer. Materials Science & Engineering A 622, p. 37.

Bajpei T., Chelladurai H., Ansari Z., 2016. Numerical investigation of transient temperature and residual stresses in thin dissimilar aluminium alloy plates. Procedia Manufacturing 5, p. 558.

Abburi Venkata K., Truman C.E., Smith D.J., Characterising residual stresses in a dissimilar metal electron beam welded plate. Procedia Engineering 130, p. 973.

Hartel U., Ilin A., Bantel C., Gibmeier J., Michailov V., 2016. Finite element modeling for the structural analysis of Al-Cu laser beam welding. Physics Procedia 83, p.1404.

Mannucci, A., Tomashchuk, I., Mathieu, A., Cicala, E., Boucheron, T., Bolot, R., Lafaye, S., 2018. Direct laser welding of pure titanium to austenitic stainless steel. Procedia CIRP 74, p. 485.

Bolot, R., Aussavy, D., Montavon, G., 2017, Application of FEM to Estimate Thermo-Mechanical Properties of Plasma Sprayed Composite Coatings, Coatings 7, p.91.

Appendix A. Bilinear stress/strain curves considered at low temperature